ELSEVIER

Journal of Hazardous Materials B137 (2006) 1608–1617

Journal of Hazardous Materials

www.elsevier.com/locate/jhazmat

Efficiency of fly ash belite cement and zeolite matrices for immobilizing cesium

S. Goñi [a,*], A. Guerrero [a], M.P. Lorenzo [b]

[a] *Instituto de Ciencias de la Construcción "Eduardo Torroja" (CSIC), C/Serrano Galvache, 4, 28033 Madrid, Spain*
[b] *Facultad de Farmacia, Universidad de San Pablo (CEU), Campus de Montepríncipe, Urbanización Montepríncipe, 28668 Boadilla del Monte, Madrid, Spain*

Received 10 March 2006; received in revised form 26 April 2006; accepted 27 April 2006
Available online 7 May 2006

Abstract

The efficiency of innovative matrices for immobilizing cesium is presented in this work. The matrix formulation included the use of fly ash belite cement (FABC-2-W) and gismondine-type Na-P1 zeolite, both of which are synthesized from fly ash of coal combustion. The efficiency for immobilizing cesium is evaluated from the leaching test ANSI/ANS 16.1-1986 at the temperature of 40 °C, from which the apparent diffusion coefficient of cesium is obtained. Matrices with 100% of FABC-2-W are used as a reference. The integrity of matrices is evaluated by porosity and pore-size distribution from mercury intrusion porosimetry, X-ray diffraction and nitrogen adsorption analyses. Both matrices can be classified as good solidify systems for cesium, specially the FABC-2-W/zeolite matrix in which the replacement of 50% of belite cement by the gismondine-type Na-P1 zeolite caused a decrease of two orders of magnitude of cesium mean Effective Diffusion Coefficient (D_e) (2.8e−09 cm^2/s versus 2.2e−07 cm^2/s, for FABC-2-W/zeolite and FABC-2-W matrices, respectively).

Keywords: Fly ash belite cement; Diffusion; Cesium; Gismondine-type Na-P1 zeolite

1. Introduction

The Portland cement is the material more extensively used in the technologies of solidification and immobilization of the toxic wastes and low and medium level wastes (LLW) and (MLW). The main solidification mechanism in the above mentioned systems is based on the precipitation of the corresponding hydroxides due to the highly alkaline pore solution of hydrated Portland cement. Nevertheless, this mechanism is not valid in the case of cesium, and, therefore, its degree of retention, in the traditional Portland cement matrices, is low and, consequently, its diffusion towards the biosphere is high [1–3].

By this, it is necessary to introduce in the matrices other components that avoid the above mentioned lacks as for example, resins with capacity of ionic exchange, fly ash, slags, zeolites, etc. [4–19].

The belite cements are good candidates for the formulation of confining matrices of radioactive liquid wastes, due to its specific characteristics. First, they present a slow hydration rate, for what the heat that is liberated is more gradual, there being avoided retraction problems, circumstance that makes it suitable for the manufacture of the above mentioned matrices. Secondly, during its hydration minims amounts of $Ca(OH)_2$ are produced, assuring a good durability in the aggressive atmospheres in which expansive reactions with $Ca(OH)_2$ could take place, as it is the case of the attack by sulphates, present in great amount in the radioactive liquid wastes [20–26].

The reactive fly ash belite cements (FABC) obtained by means of low energy processes constitute an alternative to traditional Portland cement, no single by the potentiality of its technological applications and durability, but, in addition, by the advantages of the manufacture process. These advantages then suppose a sustainable and eco-efficient alternative with reduction of the environmental impact: the temperature of synthesis is reduced drastically (800 °C versus 1450 °C); the CO_2 emission during the process of the furnace, being able to arrive at emission 0; and a waste is eliminated and the associated landfill. The expectations of demand of energy in a near future (the

* Corresponding author. Fax: +34 913020700.
E-mail addresses: sgoni@ietcc.csic.es (S. Goñi), aguerrero@ietcc.csic.es (A. Guerrero), pazloga@ceu.es (M.P. Lorenzo).

0304-3894/$ – see front matter © 2006 Elsevier B.V. All rights reserved.
doi:10.1016/j.jhazmat.2006.04.059

world-wide fly ash production is around 600 million tonnes) will imply serious environmental problems derived from their storage. Everything which, it has an important repercussion, in addition, economic by the reduction in price of implied costs.

This cement is obtained after a hydrothermal activation of fly ash, and is constituted mainly by the phase a'_L of bicalcium silicate [27–29].

The aim of this work is to study the efficiency for immobilizing cesium of belite cement and zeolite. Both cement and zeolite will be synthesized in our laboratory from industrial by-products like fly ash of the coal combustion, contributing therefore, from the point of view of the waste management to the elimination of these by-products and their landfills; to the preservation of the natural resources and to its revaluation and incorporation in the market.

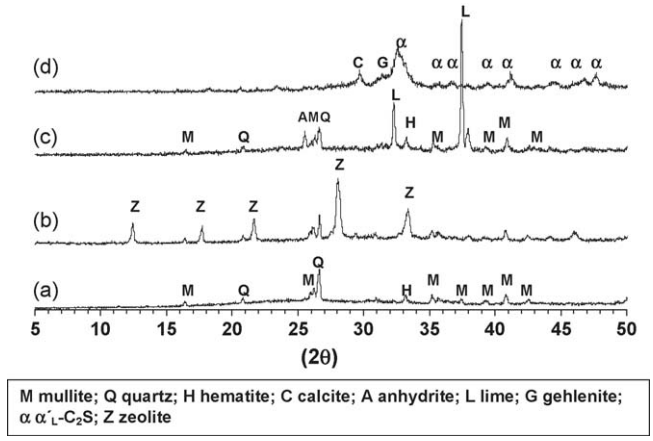

Fig. 1. X-ray diffraction patterns of the starting materials: (a) fly ash class F (FA-0); (b) zeolite type gismondine; (c) fly ash class C (FA-2); (d) fly ash belite cement FABC-2-W.

2. Experimental

2.1. Synthesis of fly ash belite cement and zeolite

Two Spanish coal fly ash, ASTM class F and C, denominated FA-0 and FA-2, respectively, were used as secondary raw materials. Gismondine-type Na-P1 zeolite was synthesized from FA-0, which was hydrothermally treated at 150 °C in an alkaline solution 1 M NaOH, according to the procedure described in reference [19] but with the following differences: solution-to-fly ash ratio of 3:1 by weight instead of 10:1; heating at 150 °C with stirring for 2 h instead of 12 h. The solid phase was washed three times with demineralized water, and dried to a constant weight at 50 °C. The main objective of these changes was to increase the efficiency of the zeolite synthesis process by using the maximum amount of fly ash or minimum amount of alkaline solution and minimum heating time. For that, different heating time: 2, 4 and 6 h and solution-to-fly ash ratio: 3:1, 5:1 and 10:1 were explored. The temperature was fixed at 150 °C because at higher values zeolite analcime-C-type is formed, which has lower selectivity for cesium than gismondine, as was concluded in a previous work [19]. The XRD characterization results showed that gismondine-type Na-P1 zeolite is formed when the solution-to-fly ash ratio was 3:1 and at the minimum heating time of 2 h (Fig. 1).

Fly ash belite cement, denominated FABC-2-W, was synthesized from FA-2 by the hydrothermal-calcination route

Table 1
Chemical composition of the starting fly ashes and FABC-2-W (% by weight)

	LOI[a]	CaO	SiO_2 (total)	Fe_2O_3	Al_2O_3	MgO	SO_3	Na_2O	K_2O	SiO_2[b] (reactive)	BET (m^2/g)
A-0	5.6	4.6	48.9	7.5	26.8	1.9	–	0.7	3.7	35.8	0.79
FA-0	4.0	32.0	32.8	4.2	19.3	2.2	2.8	0.44	1.6	25.2	3
FABC-2 W	1.4	48.3	28.7	2.3	15.2	1.4	1.7	0.25	0.5	28.6	6.4

[a] LOI, loss on ignition.
[b] Silica reactive according to Spanish standard UNE-80-224.

Table 2
Proves carried out for the mix design of the matrices

Zeolite–FABC-2-W (g)	CsCl solution/mixture			
	0.9	1	1.1	1.2
70–30	No workability	Good workability No hardened	Good workability No hardened	Good workability No hardened
60–40	No workability	Good workability No hardened	Good workability No hardened	Good workability No hardened
50–50	No workability	Good workability Hardened	Good workability Hardened	Good workability No hardened
40–60	No workability	Small workability Hardened	Good workability Hardened	Good workability No hardened
0–100	No workability	Small workability Hardened	Good workability Hardened	Good workability Hardened

described in a preliminary paper [27]. The chemical and mineralogical compositions of FA-0, FA-2 and FABC-2-W appeared in Table 1 and Fig. 1, respectively.

2.2. Fabrication of matrices: mix design

For the mix design of matrices, a preliminary optimization study was carried out by using 10 g of a mixture of zeolite and FABC-2-W cement in proportions ranging from 0:100 to 70:30 and CsCl solution to solid mixture ratios ranging from 0.9 to 1.2. The solidification of mixtures was observed after a curing period of 7 days at 60 °C. As can be seen in Table 2, for waste solution to solid ratio values lower than 1.1, the workability is very low, whereas for values higher than 1.1, the mixtures did not harden. The optimum zeolite/cement ratio was 50:50, for more zeolite amount the mixture not hardened.

Matrices were fabricated without and with a 0.1 M CsCl solution, FABC-2-W and zeolite in the following proportions (by weight of mix): solution/cement/zeolite: 52.4/23.8/23.8. After mixing, samples were molded into cylinders of 5 cm × 10 cm and demolded after 7 days of curing at 60 °C and >95% relative humidity. Equivalent matrices were fabricated with plain FABC-2-W as reference. Analytical reagent grade CsCl, was used to prepare the solution. The criteria for the formulation of matrices were the following: maximum volume of CsCl solution to be immobilized and maximum zeolite to FABC-2-W ratio.

2.3. Leaching test

The leaching test was the ANSI/ANS-16.1-1986 [30]. The leachant was demineralised water with a conductivity <5 μΩ/cm in which the specimens, with a volume of leachant to external geometric surface area of the specimen (196.35 cm^2) ratio of 10 cm, were immersed in individual plastic containers at the temperature of 40 °C. The leachate analyses were carried out on duplicate specimens.

2.3.1. Test parameters

A considerable amount of experimental data obtained from the samples, which maintained their dimensional integrity during leaching, indicated that internal bulk diffusion is the most likely rate-determining mechanism during the initial phases of the leaching process. Although additional mechanisms probably do occur to some degree, they are more likely to become rate-determining only during later ages of leaching (19, 47 and 90 days). Thus, the recommended data handling procedure of the standard is permissible, due to simplification of mass-transport theory (second Fick law at non-stationary state), for the purpose of classifying and ranking solidified wastes, according to leachability. The solution of the mass-transport equations (second Fick law), for a specimen that may be considered as a semi-infinite medium, permit the effective diffusivity to be computed by:

$$D_e = \pi \left[\frac{(c_n/C_o)}{(\Delta t)_n}\right]^2 \left[\frac{V}{S}\right]^2 T \quad (1)$$

$$T = \left[\frac{1}{2}(t_n^{1/2} + t_{n-1}^{1/2})\right]^2 \quad (2)$$

where c_n is the activity or concentration released from the specimen during the nth leaching interval; C_o is the total activity or concentration of a given ion at the beginning of the first leaching interval; $(\Delta t)_n$ is the duration of the nth leaching interval in seconds; V is the volume of the specimen in cm^3; S is the geometric surface area of the specimen in cm^2; and, T is the cumulative leaching time representing the "mean time" of the nth leaching interval for a semi-infinite medium.

Generally, this method for calculating "D_e" is valid up to 5 days of leaching time (abbreviated test), where diffusion is the rate-determining mechanism. At this point in the test, the specimen acts like a semi-infinite medium. From 5 days, the specimens, generally, acts like a finite medium, being the cumulative fraction leached higher than 20%, and other methods to calculate "D" must be used. So, for example a graphical method or interpolation, from which the parameter "G" can be obtained, in this case:

$$D_e = G\frac{d^2}{(\Delta t)_n} \quad (3)$$

where d is the diameter of the specimen in centimeter, and G a dimensionless factor.

As far as the leachability index "L" is concerned, it is a normalization factor, which is related to the specific material tested:

$$L = \log\left(\frac{\beta}{D_e}\right) \quad (4)$$

where β is a defined constant (1.0 cm^2/s). "L" also depends on the leaching conditions and the leachant renewal schedule. Leachabilty studies, therefore, consider all these variables and the results are applicable only to cases where all these factors are the same within certain error ranges.

2.4. Equipments

The cesium concentration was determined by optical emission spectrometry (OES) with inductively coupled plasma (ICP) by means of a Perkin-Elmer Optima 3300 D/V. XRD analyses were recorded on a Philips PW 1730 diffractometer making use of a graphite monochromator and Cu $K\alpha_1$ radiation. Porosity and pore-size distribution of matrices were investigated by mercury intrusion porosimetry carried out with a Micromeritics Pore Size 9310. SEM analysis was performed with an Jeol 5400 instrument equipped with an energy dispersive X-ray spectroscopy module (EDS) Oxford ISIS model. Metallized samples were prepared with carbon sputtering. SEM/EDX semiquantitative analyses were made at 20 KV and a reference current of 300 μA on powder samples. The EDX microanalysis have been carried out in spot mode over each different crystalline phase, being the limit detection of 0.2%. Specific surface area measurements were made with the multipoint BET technique using a Micromeritics ASAP 2010 analyzer, previous sample degasification at 50 °C for 24 h up to a pressure of 5 μm Hg and N_2 gas as the adsorptive. Specific surface area values were calculated from

the isotherm data using the Brunauer–Emmett–Teller (BET) [31] equation in a relative pressure range of 0.003–0.3. Pore size distributions were found with the Barret–Joyner–Halenda (BJH) method [32]. For the BET surface area and pore-size distribution analysis, monolithic pieces of about 7 mm were previously dried at room temperature in desiccators with silica gel, up to a constant weight, to eliminate free water (evaporable water) and then about 0.5 g of sample was degasified at 50 °C (to prevent decomposition of C–S–H gel) under vacuum up to reach 5 μm Hg pressure. In the case of X-ray diffraction analysis, a part of sample was grounded to particle size in the range of 75 μm and dried at room temperature in desiccators with silica gel, up to a constant weight.

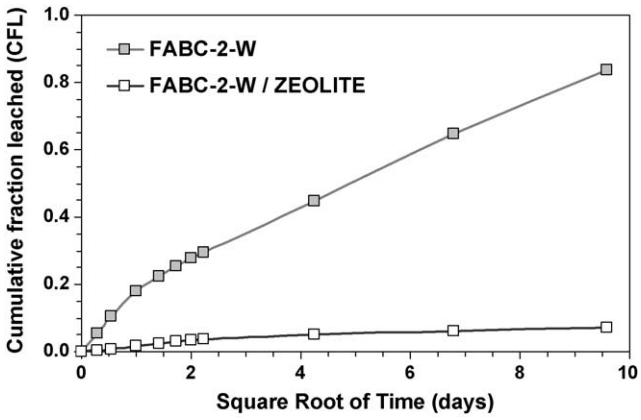

Fig. 2. Cumulative fraction leached (CFL) of cesium versus the square root of time.

3. Results and discussion

3.1. Characterization of starting materials

The chemical compositions of starting fly ashes and FABC-2-W, determined according to the Spanish standard UNE-EN 196-2, are given in Table 1. The FA-0 is in accordance with the requirements of ASTM class F and the EN-UNE 450 specifications: $SiO_2 + Al_2O_3 + Fe_2O_3$ content of over 70% and a low CaO content. On the contrary, the FA-2 is in accordance with the requirements of ASTM class C specifications: $SiO_2 + Al_2O_3 + Fe_2O_3$ content lower than 70% and high CaO content; its CaO/SiO_2 molar ratio is 1. The majority crystalline phases in the starting FA-0 (Fig. 1(a)) were quartz (α-SiO_2), mullite ($Al_6Si_2O_{13}$) and hematite (α-Fe_2O_3); the amorphous halo between 15 and 35 in the 2θ angular zone corresponds to the vitreous component of fly ash. The XRD pattern of gismondine-type Na-P1 zeolite ($Na_6Al_6Si_{10}O_{32}\cdot 12H_2O$) obtained from FA-0 can be seen in Fig. 1(b).

In the case of FA-2 (Fig. 1(c)), beside mullite and quartz, free lime (CaO) and anhydrite ($CaSO_4$) are present. The anhydrous FABC-2-W, obtained from FA-2 (Fig. 1(d)), showed broad reflections appeared at 32–33 (2θ) angular zone, which correspond to α'_L-Ca_2SiO_4 belite variety of poor crystallinity; traces of gehlenite ($Ca_2Al_2SiO_7$) appeared; the absence of free lime suggested a 100% of reaction. Calcite content was 1.1% (determined from thermogravimetric analysis).

3.2. Leaching analyses

The effective diffusion coefficient (D_e), together with other measured parameters for each leaching interval are given in Table 3, for the two matrices studied. The cumulative fraction leached of cesium is presented in Fig. 2. As can be seen, the matrix fabricated with FABC-2-W/zeolite has values of cesium cumulative fraction leached (CFL) near two orders of magnitude lowers than those of the plain FABC-2-W matrix. The mean effective diffusion coefficient (D_e), up to 5 days of leaching (abbreviated test), is 2.2e−07 cm^2/s for FABC-2-W matrix and that of FABC-2-W/zeolite matrix, 2.8e−09 cm^2/s. The kinetic of the process is slower at longer leaching time, decreasing the corresponding D_e values after 90 days of leaching up to 4.2e−8 and 1.1e−10 cm^2/s, for the FABC-2-W and FABC-2-W/zeolite matrices, respectively. In the later case, the decrease of D_e can be attributed to the formation of a carbonated film which cover the external surface of matrix (see Fig. 4).

Table 3
Leaching analyses of FABC-2-W and FABC-2-W/ZEOLITE matrices

Matrix	FABC-2-W (C_o = 6.97 g/Kg)						FABC-2-W/ZEOLITE (C_o = 6.81 g/Kg)					
$(\Delta t)_n$ (s)	c_n (g/kg)	F_n c_n/C_o	F $\sum c_n/C_o$	D_e (cm^2/s)	L	R_n $F_n/(\Delta t)_n$	c_n (g/kg)	F_n c_n/C_o	F $\sum c_n/C_o$	D_e (cm^2/s)	L	R_n $F_n/(\Delta t)_n$
7.2e03	0.39	0.056	0.056	3.4e−07	6.5	7.7e−06	0.015	0.0022	0.0022	5.4e−10	9.3	3.1e−07
1.8e04	0.35	0.050	0.11	3.6e−07	6.4	2.8e−06	0.023	0.0033	0.0055	1.6e−09	8.8	1.8e−07
6.1e04	0.50	0.072	0.18	2.2e−07	6.6	1.2e−06	0.068	0.0099	0.016	4.3e−09	8.4	1.6e−07
8.6e04	0.33	0.047	0.23	1.2e−07	6.9	5.5e−07	0.053	0.0078	0.023	3.2e−09	8.5	9.0e−08
8.6e04	0.20	0.029	0.25	7.7e−08	7.1	3.4e−07	0.038	0.0055	0.029	2.8e−09	8.6	6.4e−08
8.6e04	0.15	0.022	0.28	6.1e−08	7.2	2.5e−07	0.038	0.0055	0.034	3.9e−09	8.4	6.4e−08
8.6e04	0.13	0.019	0.30	5.8e−08	7.2	2.2e−07	0.030	0.0044	0.039	3.2e−09	8.5	5.1e−08
1.1e06	1.1	0.15	0.45	5.1e−08	7.3	1.3e−07	0.083	0.012	0.051	3.4e−10	9.5	1.1e−08
2.4e06	1.4	0.20	0.65	5.6e−08	7.2	8.3e−08	0.068	0.0099	0.061	1.4e−10	9.9	4.1e−09
4.0e06	1.3	0.19	0.84	4.2e−08	7.4	4.8e−08	0.068	0.0099	0.071	1.1e−10	9.9	2.5e−09

FABC-2-W (C_o = 6.97 g/kg): mean D_e = 2.2e−07(abbreviated test), mean leachability index, L_i = 6.7 (abbreviated test), standard deviation, σ = 0.3; FABC-2-W/Zeolite (C_o = 6.81 g/kg): mean D_e = 2.8e−09 (abbreviated test), mean leachability index, L_i = 8.6 (abbreviated test), standard deviation, σ = 0.3; C_o is the initial Cs concentration, expressed as g of Cs/kg of matrix.

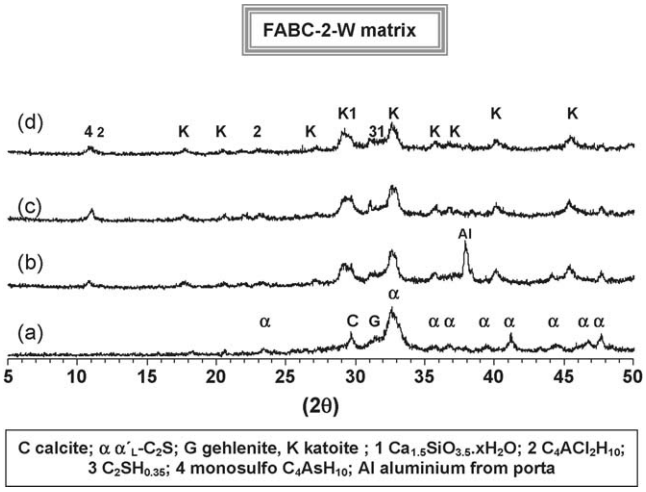

Fig. 3. X-ray diffraction patterns of: (a) anhydrous FABC-2-W; (b) after 7 days of curing at 60 °C, without Cs (c)) after 7 days of curing at 60 °C, with Cs; (d) after 90 days of leaching.

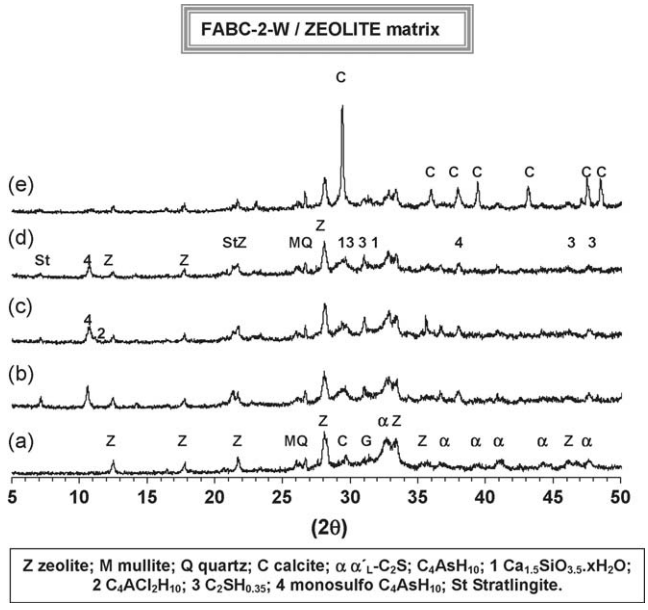

Fig. 4. X-ray diffraction patterns of: (a) anhydrous FABC-2-W/ZEOLITE mixture; (b) after 7 days of curing at 60 °C, without Cs (c)) after 7 days of curing at 60 °C, with Cs; (d) after 90 days of leaching; (e) external carbonated film.

The mean leachability index (L) is used to catalogue the efficiency of a matrix material to solidify a waste, being the value of 6 the threshold to accept a given matrix as adequate for the immobilization of nuclear wastes [30]. As it is shown in Table 3, the mean leachability index (L), during the first 5 days, is 6.7 and 8.6 for the FABC-2-W and FABC-2-W/zeolite matrices, respectively, consequently, both matrices, and specially the FABC-2-W/zeolite matrix can be catalogued as efficient materials for immobilizing cesium from nuclear wastes.

It is necessary to mention the difficulty that represents the comparison of the results of diffusion of the cesium obtained in this work with the published ones by other authors. This is due to differences in: types of leaching tests; matrix geometries and compositions; concentration of cesium; types of evaporator concentrates, temperature, etc.

Taking this into account, the effective diffusion coefficient of cesium obtained from the abbreviated test (up to 5 days), in the case of the plain belite cement matrix (2.2e−07 cm^2/s), is quite similar to those obtained for matrices fabricated by the authors with Portland cement type I-35A (2.0e−07 cm^2/s), Portland cement type IV-35A (5.9e−07 cm^2/s) and by using the same geometry of matrices, the same leaching test and the same temperature of 40 °C [3].

3.3. Characterization of matrices

3.3.1. X-ray diffraction

Figs. 3 and 4 show the changes of the X-ray diffraction patterns of plain FABC-2-W and FABC-2-W/zeolite matrices before and after leaching attack. The XRD results of equivalent matrices mixing with demineralised water instead of CsCl solution have been included for comparison.

In the case of plain FABC-2-W matrix (Fig. 3(b)), the main hydrated compounds formed were $C_2SH_{0.35}$ ($Ca_2SiO_4{\cdot}0.35H_2O$), C–S–H gel ($Ca_{1.5}SiO_{3.5}{\cdot}xH_2O$), hydrated calcium monosulpho aluminate ($Ca_4Al_2(SO_4)O_6{\cdot}10H_2O$) and katoite ($Ca_3Al_2(SiO_4)(OH)_8$). No significant changes were produced neither by the presence of CsCl solution (Fig. 3(c)) nor by the leaching attack (Fig. 3(d)).

For FABC-2-W/zeolite matrix (Fig. 4), the main differences observed in the hydrated compounds are the following: the absence of katoite; the formation of strattlingite ($Ca_2Al_2SiO_7{\cdot}8H_2O$) (from the hydration of gehlenite) and the higher intensity of $Ca_4Al_2(SO_4)O_6{\cdot}10H_2O$ reflections (see Fig. 4(b)). In the presence of CsCl solution, the intensity of the aforementioned hydrated compounds decreased; traces of the β-$Ca_4Al_2(Cl_2)O_6{\cdot}10H_2O$ appeared from the combination of chlorides with $Ca_4Al_2(SO_4)O_6{\cdot}10H_2O$. No significant changes were produced after the leaching attack (Fig. 4(d)). As it has been commented previously, an external carbonated film was formed after leaching (see Fig. 4(e)).

It should be mentioned that crystalline cesium compounds were not formed neither in the FABC-2-W nor in the FABC-2-W-zeolite matrices, suggesting that cesium is not chemically combined. Nevertheless, from the low cesium diffusion coefficient obtained for FABC-2-W-zeolite matrix, one can deduce that the zeolite is clearly a host phase for cesium which is strongly immobilized. In the case of FABC-2-W matrix, the cesium is detected mainly in the C–S–H gel (see the X-ray microanalyses of Table 4), but its degree of immobilization is clearly much lower than that of zeolite.

3.3.2. Pore structure

The differential pore size distribution and total porosity of matrices, determined from mercury intrusion porosimetry and the changes introduced by leaching attack are depicted in Fig. 5. As shown, the porosity of FABC-2-W/zeolite matrix (73% by weight) is 30% higher than that of FABC-2-W matrix (51%), with a very homogeneous pore size distribution with a maximum centred at 0.1 μm of diameter. The pore structure of this matrix

Table 4
X-ray microanalyses of starting zeolite and matrices (%atom).

		Si	Al	Fe	Ca	Na	K	S	Cs	Na/Al	Si/Ca	Al/Ca	S/Ca
Zeolite	Fig. 7(b)	0.90	0.50	0.024	0.020	0.45	0.076	0.001	-	0.9	52	28	0.07
	Fig. 7(c) mark 1	0.98	0.45	0.022	0.001	0.47	0.050	0	-	1.1	1092	502	0
FABC-2-W unleached	Fig. 8(a) mark 1	0.57	0.18	0.015	0.91	0.015	0.018	0.014	0.010	0.09	0.62	0.19	0.015
	Fig. 8(a) mark 2	0.48	0.16	0.019	1.00	0.026	0.017	0.019	0.011	0.16	0.48	0.16	0.019
	Fig. 8(b) mark 3	0.25	0.45	0.014	0.94	0.013	0.007	0.058	0.006	0.03	0.26	0.48	0.062
	Fig. 8(b) mark 4	0.28	0.45	0.011	0.81	0.010	0.010	0.020	0	0.02	0.35	0.55	0.025
	Fig. 8(c) mark 5	0.53	0.28	0.40	0.09	0.17	0.014	0	0	0.6	5.65	2.94	0
FABC-2-W leached	Fig. 9(a) mark 1	0.61	0.23	0.030	0.82	0.025	0.012	0.016	0.004	0.11	0.75	0.28	0.019
	Fig. 9(a) mark 2	0.60	0.26	0.016	0.83	0.025	0.011	0.019	0	0.09	0.73	0.31	0.023
	Fig. 9(b) mark 3	0.23	0.48	0.015	0.93	0.044	0.011	0.047	0.001	0.09	0.25	0.51	0.050
	Fig. 9(b) mark 4	0.15	0.52	0.003	1.01	0.014	0.007	0.048	0.001	0.03	0.15	0.51	0.047
FABC-2-W/Z unleached	Fig. 10(a) mark 1	0.89	0.40	0.028	0.11	0.34	0.086	0.003	0.024	0.83	8.2	3.71	0.024
	Fig. 10(b) mark 2	0.82	0.37	0.029	0.22	0.21	0.10	0.004	0.039	0.58	3.71	1.67	0.016
	Fig. 10(b) mark 3	0.26	0.31	0.025	0.98	0.06	0.025	0.038	0.014	0.20	0.27	0.32	0.039
	Fig. 10(c) mark 4	0.50	0.47	0.016	0.60	0.12	0.042	0.024	0.013	0.26	0.84	0.79	0.040
FABC-2-W/Z leached	Fig. 11(a) mark 1	0.85	0.46	0.019	0.14	0.27	0.075	0.005	0.027	0.59	5.98	3.19	0.033
	Fig. 11(b) mark 2	0.59	0.13	0.020	0.94	0.033	0.016	0.020	0.001	0.25	0.63	0.14	0.021
	Fig. 11(b) mark 3	0.28	0.46	0.018	0.86	0.051	0.011	0.060	0.005	0.11	0.32	0.54	0.070
	Fig. 11(c) mark 4	0.33	0.41	0.015	0.96	0.043	0.022	0.011	0.003	0.10	0.34	0.42	0.012

is not affected by leaching attack. In the case of FABC-2-W matrix, the mayority of pores also have diameters of 0.1 μm; the leaching caused the appearance of pores of 2.5 μm of diameter.

The high total porosity of both matrices caused a low bulk density: 1.0 and 0.83 g/mL for FABC-2-W and FABC-2-W/zeolite matrices, respectively.

The BET surface area and differential pore size distribution of matrices, obtained from nitrogen adsorption, and the changes introduced by leaching attack are depicted in Fig. 6.

The surface area of FABC-2-W/zeolite matrix (109 m^2/g) is 21% higher than that of FABC-2-W (86 m^2/g), due to the contribution of starting zeolite (40 m^2/g) versus 6.4 m^2/g of starting cement. After leaching attack, the surface area of FABC-2-W/zeolite matrix sligthly decreased (from 109 to 102 m^2/g), whereas, in the case of FABC-2-W matrix sligthly increased (from 86 to 91 m^2/g).

The differential pore size distribution of unleached FABC-2-W/zeolite matrix showed a peak centred at about 4 nm, which

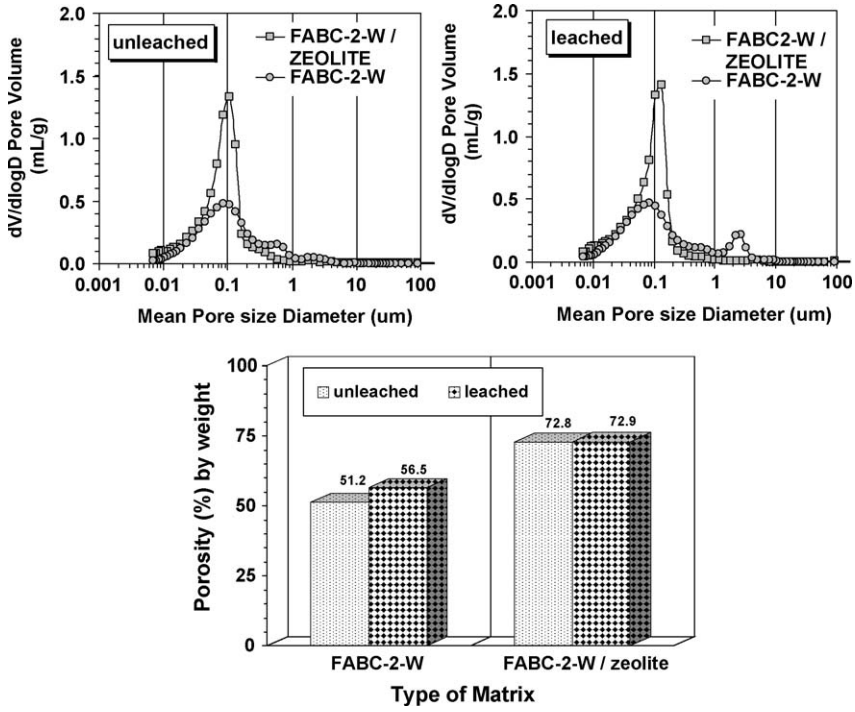

Fig. 5. Pore size distribution and porosity of matrices determined by mercury intrusion porosimetry: influence of leaching.

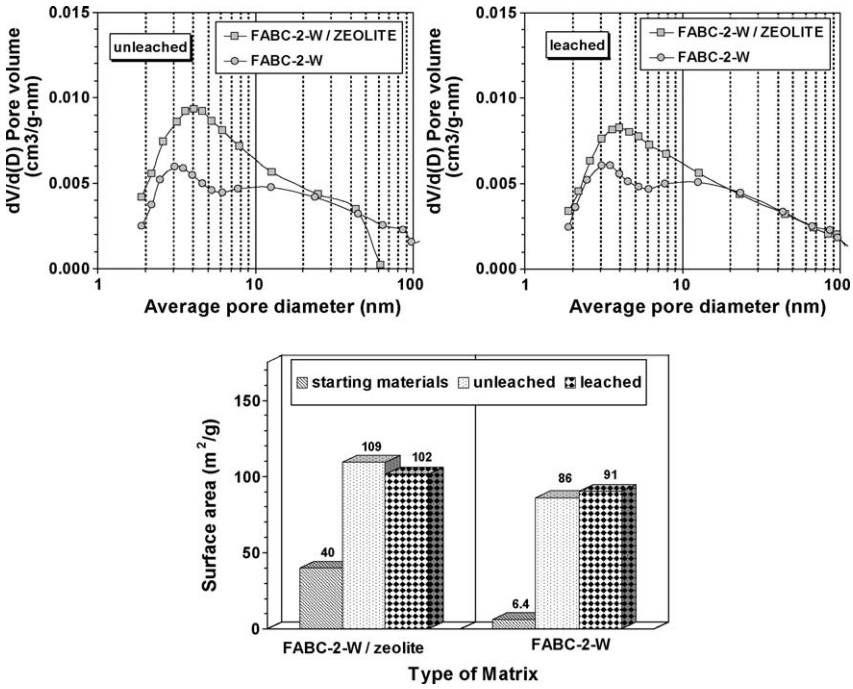

Fig. 6. Pore size distribution and BET-N_2 surface area of matrices determined by nitrogen adsorption: influence of leaching.

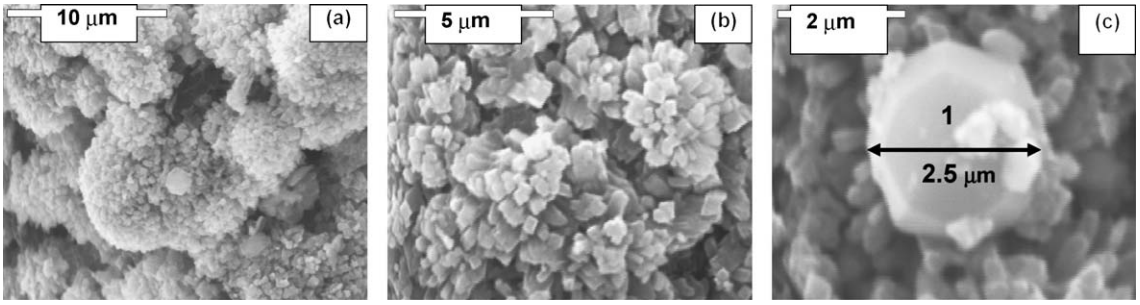

Fig. 7. SEM images of fly ash class F (FA-0) after hydrothermal treatment in NaOH at 150 °C.

indicates a much higher proportion of pore volume in pores having diameters of 4 nm. In the case of unleached FABC-2-W matrix, two maxima are detected at 3 nm and about 10 nm.

The leaching attack produced an increase in the volume of pores of diameters higher than 40 nm for the FABC-2-W/zeolite matrix.

3.3.3. Scanning electron microscopy analyses

SEM analyses were conducted on the starting zeolite (Fig. 7); unleached and leached FABC-2-W and FABC-2-W/zeolite matrices (Figs. 8–11). The percentage of the main elements analysed is given in Table 4. The zeolite obtained from FA-0 appeared in large clusters of tetragonal prisms (Fig. 7(a)), which can be seen at a higher magnification in Fig. 7(b)), large

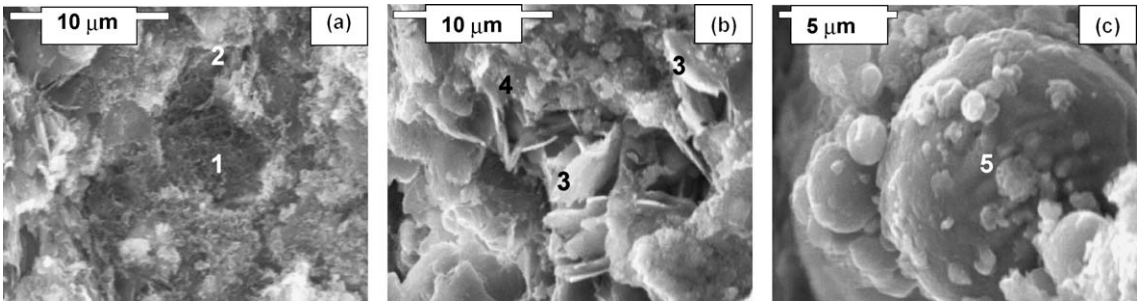

Fig. 8. SEM images of unleached FABC-2-W matrix.

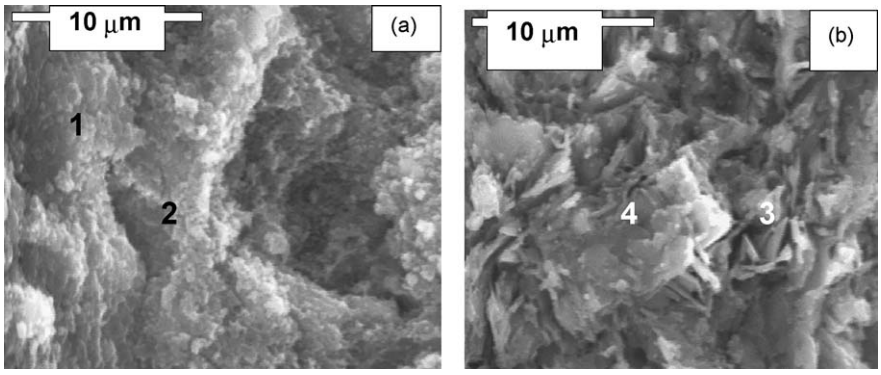

Fig. 9. SEM images of leached FABC-2-W matrix.

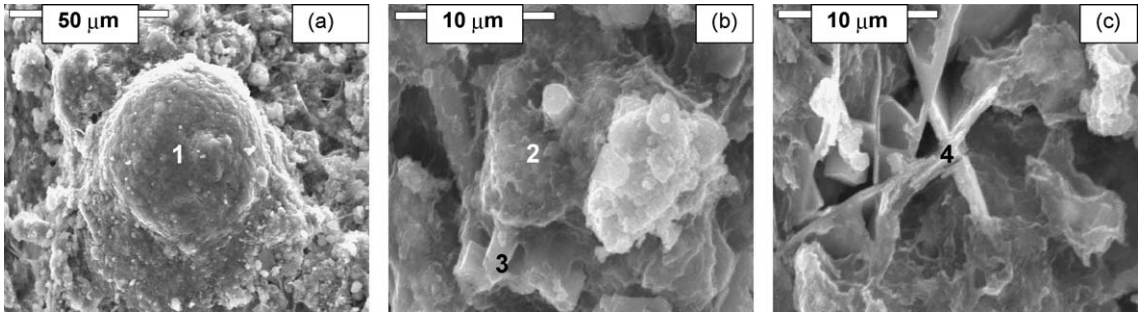

Fig. 10. SEM images of unleached FABC-2-W/zeolite matrix.

cubic crystals of gismondine-type Na-P1 zeolite were observed (Fig. 7(c)).

In the case of unleached FABC-2-W matrix (Fig. 8), fibrous C–S–H gel is detected in Fig. 8(a) marks 1 and 2, which contained considerable amount of Na, K, Fe, Al, S and Cs, their Si/Ca atom ratio were 0.62 and 0.48 for mark 1 and 2, respectively (see Table 4). Plates with high S and Al content and compositions between monosulfo and monocarbo hydrated calcium aluminate can be seen in Fig. 8(b) mark 3; small particles of mark 4 have high amount of Al and composition consistent with katoite. In Fig. 8(c), cenospheres of unreacted FA-2 can be observed. As shown in Table 4, the majority of cesium is in the C–S–H gel (Fig. 8(a)).

After leaching attack, the more relevant change is observed in the C–S–H gel morphology, which appeared more dense (Fig. 9(a)); the corresponding Si/Ca and Al/Ca atom ratios are higher compared with those of C–S–H gel of unleached FABC-2-W matrix of Fig. 8(a). This increase is caused by Ca leaching over time. The cesium content in the C–S–H gel also decreased as a result of leaching. The plates of high S and Al content appeared deformed in Fig. 9(b) as a result of a partial dissolution caused by leaching. That dissolution could be the reason of increasing the amount of pores in the range of 2.5 μm of diameters (see Fig. 5).

In the case of unleached FABC-2-W/zeolite matrix (Fig. 10), cenospheres covered by small zeolite crystals appeared in Fig. 10(a); zeolite also appeared like in (b) mark 2, in which the content of cesium is the higher (see Table 4).

Plates rich in Ca corresponds to mark 3 in Fig. 10(b) and plates rich in Al (Fig. 10(c) mark 4) appeared bigger than those of FABC-2-W matrix of Fig. 8(b). The cesium content of zeolite particles almost did not change after leaching attack (Fig. 11(a) mark 1); more remarkable effect of leaching is that showed in Fig. 11(c), where small plates of similar composi-

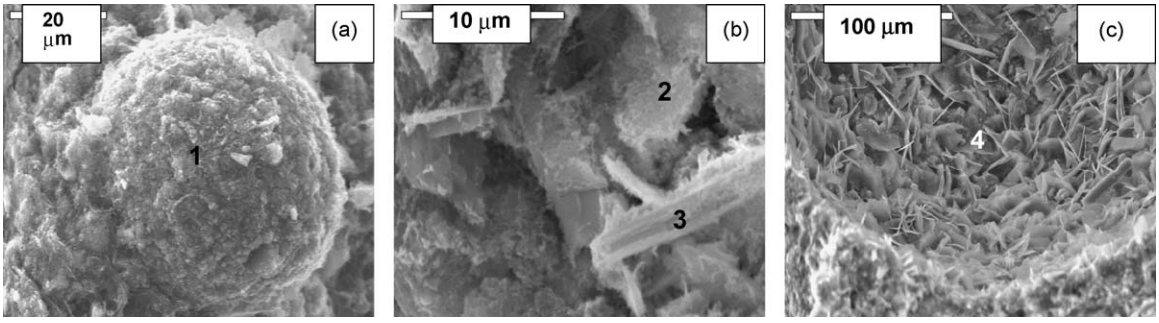

Fig. 11. SEM images of leached FABC-2-W/zeolite matrix.

tion than that of mark 3 in Fig. 11(b) appeared growing in a big pore.

4. Conclusions

- Both matrices studied can be classified as good solidify systems for cesium, according to the leaching test ANSI/ANS-16.1-1986. Specially the FABC-2-W/zeolite matrix in which the replacement of 50% of belite cement by the gismondine-type Na-P1 zeolite caused a decrease of two orders of magnitude of cesium mean Effective Diffusion Coefficient (D_e) (2.8e−09 cm^2/s versus 1.8e−07 cm^2/s, for FABC-2-W/zeolite and FABC-2-W matrices, respectively).
- According to the EDX microanalyses, in the case of plain belite cement matrix (FABC-2-W), cesium is mainly trapping by C–S–H gel and by zeolite for FABC-2-W/zeolite matrix.
- The pore size distribution (determined by mercury intrusion porosimetry) of both matrices is very homogeneous, having practically all pores diameters of 0.1 μm. It should be mentioned the high total open porosity of both matrices but specially that of the zeolite matrix (73 and 51%), which is caused by the high contain of liquid waste. In spite of that, cesium is efficiently retained.
- The high surface area of both matrices, and especially zeolite matrix are due to the C–S–H gel (interlayer spaces) and zeolite cavities, in which cesium is mainly trapped. Therefore, the surface area of a matrix could be another valuable tool for evaluating its efficiency as immobilization system.
- The high resistance of matrices to the leaching attack at 40 °C is manifested by the small changes in their pore structure and surface area.

Acknowledgement

Funding for the present research was provided by the CAM under Project GR/AMB/0452/2004.

References

[1] C.E. McCulloch, A.A. Rahman, M.J. Angus, F.P. Glasser, Immobilization of cesium in cement containing reactive silica and pozzolans, in: G.G. Wicks, W.A. Ros (Eds.), Advances in Ceramics, vol. 8, Nuclear Waste Management, 1984, pp. 413–428.

[2] A. Guerrero, S. Goñi, M^a.S. Hernández, M^a.P. Lorenzo, Alkalinity of cement-based materials and their confine characteristics, sodium and potassium leaching behaviour, in: Proceedings of Solid and Liquid Wastes: Their Best Destination (II). vol. II, 1994, ISBN 84-88233-16-7, pp. 455–464.

[3] A. Guerrero, M^a.S. Hernández, S. Goñi, Cemented materials in the LLW and MLW Spanish disposal, Materiales de Construcción 49 (1999) 31–39.

[4] M. Atkins, F.P. Glasser, J.J. Jack, Zeolite P in cements: its potential for immobilizing toxic and radioactive waste species, Waste Manage. 15 (2) (1995) 127–135.

[5] S. Bagosi, L.J. Csetenyi, Immobilization of caesium-loaded ion exchange resins in zeolite-cement blends, Cem. Concr. Res. 29 (1999) 479–485.

[6] A.R. Brough, A. Katz, G.K. Sun, L.J. Struble, R.J. Kirkpatrick, J.F. Young, Adiabatically cured, alkali-activated cement-based wasteforms containing high levels of fly ash: formation of zeolites and Al-substituted C-S-H, Cem. Concr. Res. 31 (2001) 1437–1447.

[7] A. Kumar, S. Komarneni, D.M. Roy, Diffusion of Cs^+ and Cl^- trough sealing materials, Cem. Concr. Res. 17 (1) (1987) 153–160.

[8] S.L. Hoyle, M.W. Grutzeck, Incorporation of cesium by hydrating calcium aluminosilicates, J. Am. Ceram. Soc. 72 (10) (1989) 1938–1947.

[9] J. LaRosa, S. Kwan, M.W. Grutzeck, Zeolite formation in class F fly ash blended cement pastes, J. Am. Ceram. Soc. 75 (1992) 1574–1580.

[10] G. Nicolas, N. Lequeux, S. Prene, P. Boch, Zeolite cement blend for trapping radioactive waste, in: G. Grieve, G. Owens (Eds.), Proceedings of the 11th International Congress on the Chemistry of Cement (ICCC) Cement's Contribution to the Development in the 21st Century, Durban, South Africa, 2003, pp. 2199–2204.

[11] W. Ma, P.W. Brown, S. Komarneni, Characterization and cation exchange properties of zeolites synthesized from fly ashes, J. Mater. Res. 13 (1) (1998) 3–7.

[12] T. Nishi, M. Matsuda, K. Chino, M. Kikuchi, Reduction of cesium leachability from cementitous resin forms using natural acid clay and zeolite., Cem. Concr. Res. 22 (2–3) (1992) 387–392.

[13] P. Bosch, D. Caputo, B. Liguori, C. Colella, Safe trapping of Cs in heat-treated zeolite matrices, J. Nucl. Mater. 324 (2004) 183–188.

[14] I. Plecas, Leaching of Cs from spent ion exchange resins in cement–bentonite clay matrix, Acta Chim. Slov. 50 (2003) 593–596.

[15] I. Plecas, S. Dimovic, I. Smiciklas, Utilization of bentonite and zeolite in cementation of dry radioactive evaporator concentrate, Prog. Nucl. Energy, doi:10.1016/j.pnucene.2005.12.001.

[16] A.M. El-Kamash, M.R. El-Naggar, M.I. El-Dessouky, Immobilization of cesium and strontium radionuclides in zeolite-cement blends, J. Hazard. Mater., doi:10.1016/j.jhazmat.2005.12.020.

[17] A. Fernandez-Jimenez, D.E. Macphee, E.E. Lachowski, A. Palomo, Immobilization of cesium in alkaline activated fly ash matrix, J. Nucl. Mater. 346 (2005) 185–193.

[18] H. Nugteren, J. Davidovits, D. Antenucci, C. fernández Pereira, X. Querol, Geopolimerization of fly ash, in: Proceedings of World of Coal Ash, Lexington, Kentucky, USA, April 11–15, 2005.

[19] R. Peña, A. Guerrero, S. Goñi, Immobilization of Cs, Cd, Pb and Cr by synthetic zeolites from Spanish coal-low-calcium-fly ash, Fuel 85 (2006) 823–832.

[20] A. Guerrero, S. Goñi, A. Macías, Durability of new fly ash-belite Cement mortars in sulfated and chloride medium, Cem. Concr. Res. 30 (8) (2000) 1231–1238.

[21] M^a.S. Hernández, A. Guerrero, S. Goñi, M^a.P. Lorenzo, Effect of the temperature on the leaching performance of the cement-based immobilization systems, Sulfate and chloride behavior, Cem. Concr. Res. 26 (4) (1997) 515–524.

[22] A. Guerrero, M^a.S. Hernández, S. Goñi, Reaction between simulated sulfate radioactive liquid waste and cement based materials, in: Proceedings of the 10th International Congress on the Chemistry of Cement, Perfomance and Durability of Cementitious Materials, IV: 4iv024, 1997.

[23] A. Guerrero, M^a.S. Hernández, S. Goñi, Durability of cement-based materials in simulated radioactive liquid waste: effects of phosphate, sulphate and chloride ions, J. Mater. Res. 13 (8) (1998) 2151–2160.

[24] A. Guerrero, M^a.S. Hernández, S. Goñi, The role of the fly ash pozzolanic activity in simulated sulphate radioactive liquid waste, Waste Manage. 20 (2000) 51–58.

[25] A. Guerrero, S. Goñi, M^a.S. Hernández, Thermodynamic solubility constant of $Ca(OH)_2$ in simulated radioactive sulfate liquid waste, J. Am. Ceram. Soc. 83 (4) (2000) 882–888.

[26] A. Guerrero, M^a.S. Hernández, S. Goñi, Effect of simulated radioactive liquid waste on the microstructure of cementitious materials: portlandite orientation and saturation factors in the pore solution, J. Am. Ceram. Soc. 83 (11) (2000) 2803–2808.

[27] A. Guerrero, S. Goñi, I. Campillo, A. Moragues, Belite cement clinker from coal fly ash of high Ca content. Optimization of synthesis parameters, Environ. Sci. Technol. 38 (12) (2004) 3209–3213.

[28] S. Goñi, A. Guerrero, A. Moragues, M.F. Tallafigo, I. Campillo, J. Sánchez, A. Porro, New Belite Cement Clinkers from Fly ash of Coal Combustion of High Ca Content. Spanish Patent No ES 2,223,275 A1, published 16, February, 2005.

[29] A. Guerrero, S. Goñi, A. Moragues, J.S. Dolado, Microstructure and mechanical performance of belite cements from high calcium coal fly ash, J. Am. Ceram. Soc. 88 (7) (2005) 1845–1853.
[30] ANSI/ANS-16.1986, Measurement of the leachability of solidified low-level radioactive wastes by a short-term test procedure, ANSI/ANS 16.1, American Nuclear Society (1986).
[31] S. Brunauer, P.H. Emmett, E. Teller, Adsorption of gases in multimolecular layers, J. Am. Chem. Soc 62 (1940) 723.
[32] E.P. Barret, L.G. Joyner, P.P. Halenda, The determination of pore volume and area distributions in porous substances, J. Am. Chem. Soc. 73 (1951) 373–381.